

Effect of lattice distortion on spin admixture and quantum transport in organic devices with spin-orbit coupling

Ying Wang(王莹), Dan Li(李丹), Xinying Sun(孙新英), Huiqing Zhang(张惠晴), Han Ma(马晗), Huixin Li(李慧欣), Junfeng Ren(任俊峰), Chuankui Wang(王传奎), and Guichao Hu(胡贵超)

Citation: Chin. Phys. B, 2024, 33 (**7**): 077101. DOI: 10.1088/1674-1056/ad35ae
Journal homepage: http://cpb.iphy.ac.cn; http://iopscience.iop.org/cpb

What follows is a list of articles you may be interested in

Angle-resolved photoemission study of NbGeSb with non-symmorphic symmetry

Huan Ma(马欢), Ning Tan(谭宁), Xuchuan Wu(吴徐传), Man Li(李满), Yiyan Wang(王义炎), Hongyan Lu(路洪艳), Tianlong Xia(夏天龙), and Shancai Wang(王善才)
Chin. Phys. B, 2024, 33 (**2**): 027102. DOI: 10.1088/1674-1056/ad0ccf

Design of sign-reversible Berry phase effect in 2D magneto-valley material

Yue-Tong Han(韩曰通), Yu-Xian Yang(杨宇贤), Ping Li(李萍), and Chang-Wen Zhang(张昌文)
Chin. Phys. B, 2023, 32 (**9**): 097101. DOI: 10.1088/1674-1056/acd920

Highly anisotropic Dirac fermion and spin transportproperties in Cu-graphane

Chao Wu(吴超), Lichuan Zhang(张礼川), Lin Xia(夏霖), Dong Hao(郝东), Shiqi Li(李仕琪), Lizhi Zhang(张礼智), Yuee Xie(谢月娥), and Yuanping Chen(陈元平)
Chin. Phys. B, 2023, 32 (**8**): 087104. DOI: 10.1088/1674-1056/accff1

Rashba spin-orbit coupling induced rectified currents in monolayer graphene with exchange field and sublattice potential

Liang Chen(陈亮), Feng Li(李峰), and Xiao-Ming Ding(丁晓明)
Chin. Phys. B, 2023, 32 (**8**): 087103. DOI: 10.1088/1674-1056/acc932

Coexistence of giant Rashba spin splitting and quantum spin Hall effect in H-Pb-F

Wenming Xue(薛文明), Jin Li(李金), Chaoyu He(何朝宇), Tao Ouyang(欧阳滔), Xiongying Dai(戴雄英), and Jianxin Zhong(钟建新)
Chin. Phys. B, 2023, 32 (**3**): 037101. DOI: 10.1088/1674-1056/aca7eb

---

Effect of lattice distortion on spin admixture and quantum transport in organic devices with spin–orbit coupling

Ying Wang(王莹), Dan Li(李丹), Xinying Sun(孙新英), Huiqing Zhang(张惠晴), Han Ma(马晗), Huixin Li(李慧欣), Junfeng Ren(任俊峰), Chuankui Wang(王传奎), and Guichao Hu(胡贵超)[†]

School of Physics and Electronics, Shandong Normal University, Jinan 250358, *China*

(Received 21 December 2023; revised manuscript received 4 March 2024; accepted manuscript online 20 March 2024)

With an extended Su–Schrieffer–Heeger model and Green's function method, the spin–orbit coupling (SOC) effects on spin admixture of electronic states and quantum transport in organic devices are investigated. The role of lattice distortion induced by the strong electron–lattice interaction in organics is clarified in contrast with a uniform chain. The results demonstrate an enhanced SOC effect on the spin admixture of frontier eigenstates by the lattice distortion at a larger SOC, which is explained by the perturbation theory. The quantum transport under the SOC is calculated for both nonmagnetic and ferromagnetic electrodes. A more notable SOC effect on total transmission and current is observed for ferromagnetic electrodes, where spin filtering induced by spin-flipped transmission and suppression of magnetoresistance are obtained. Unlike the spin admixture, a stronger SOC effect on transmission exists for the uniform chain rather than the organic lattices with distortion. The reason is attributed to the modified spin-polarized conducting states in the electrodes by lattice configuration, and hence the spin-flip transmission, instead of the spin admixture of eigenstates. This work is helpful to understand the SOC effect in organic spin valves in the presence of lattice distortion.

Keywords: organic spintronics, spin–orbit coupling, spin admixture, quantum transport

PACS: 71.70.Ej, 73.43.Qt, 05.60.Gg **DOI:** 10.1088/1674-1056/ad35ae

1. Introduction

Organic spintronics has attracted much attention in the last few decades because of the merits of organic materials in spintronics, such as low-cost synthesis, long spin relaxation time, diversity of carriers, and controllable spin polarization at interfaces.[1–5] Various organic spintronic devices have been designed and measured, including organic spin valves, organic spin filters, and organic spin diodes.[6–9] A distinct characteristic of organic devices is the intrinsic strong electron–lattice (e-l) interaction in organics. The e-l interaction may cause lattice distortion, either in the ground or charged state, and further modifies the transport property of the device, e.g., dimerization induced inversion of magnetoresistance (MR),[10] polaron induced conducting switch[11] and negative differential resistance.[12]

Spin–orbit coupling (SOC) in organics and its underlying role in electronic transport are attractive but challenging issues. Due to the light-atom component, the SOC in organics has usually been neglected in past studies. However, recent reports have demonstrated that the SOC in organics cannot be ignored simply in several cases. For example, some organic molecules contain heavy atoms,[13–15] such as Al in tris-(8-hydroxyquinoline) aluminum (Alq_3), S in sexithienyl (T6) and Cu in copper phthalocyanine (CuPc).[16] Moreover, the strength of the SOC in organics may be modified by molecular deformation.[17–21] It has been reported that the SOC in biphenyls is increased by four orders of magnitude as the torsion angle between the two benzene rings changes.[16] This provides a prerequisite for exploring the SOC effect in organic devices. The related SOC effect in organics has triggered increasing interest, including topological insulators and spin Hall effect.[22–25] Moreover, it is known that SOC is an important factor for electronic spin relaxation in spintronic devices. Experimental study has demonstrated that when atoms with atomic number larger than S are present in organics, the SOC will become the dominant reason for spin relaxation.[26] Thus, the exploration of the SOC effect in organics is helpful to understand the related spin transport properties, such as spin valves, especially in a situation where the SOC cannot be neglected simply.

The presence of SOC will mix the up- and down-spins in an electronic eigenstate, and the spin is no longer a good quantum number. Spin admixture of frontier molecular orbitals in several organic molecules has been investigated by Yu with an *ab-initio* method,[16] which reflects the strength of the SOC to some extent. The spin admixture in electronic states will further induce spin-flip transport in the device. For instance, the SOC leads to a spin-flip conductance as reported in finite carbon nanotubes and molecular junctions.[27,28] Spin pumping experiments in poly (3-alkylthiophene) polymer films have shown that a polymer with a higher degree of distortion leads to a larger spin mixing conductivity.[29] The SOC in chiral molecules is also found to be significant and plays a crucial role in the enhancement of spin polarization during electronic transport.[30–34]

[†]Corresponding author. E-mail: hgc@sdnu.edu.cn

© 2024 Chinese Physical Society and IOP Publishing Ltd

As mentioned earlier, the change of molecular conformation may modify the SOC strength in organics. The reported structural deformation in previous theoretical studies is limited to the change of molecular angles or chemical substitution in heterocyclic molecules.[17–21] In organic polymers, a fundamental structural deformation is the lattice dimerization or polaron lattice distortion induced by the strong e-l interaction. These lattice distortions exist universally in organics, which may even bring novel effects for spin transport related to the SOC, such as the oscillation spin Hall effect in organic ladders induced by polaron and bipolaron transport.[23,24] However, the questions of how such lattice distortions modify the SOC and their potential roles in quantum transport have not been fully addressed and clarified clearly. In this paper, we investigate the spin admixture of the frontier eigenstates in one-dimensional organic chains, where both the Rashba SOC and e-l interaction are included. Then, by sandwiching the organic chain between two nonmagnetic or ferromagnetic electrodes, the spin-dependent transport properties of organic devices with these two interactions are explored. This paper is organized as follows. In Section 2, the model and calculation method are introduced. In Section 3, we discuss the results and analyze the underlying physics. Finally, a brief conclusion is given in Section 4.

2. Model and method

We first consider a one-dimensional organic chain including the SOC and e-l interaction. The organic chain is described by an extended Su–Schrieffer–Heeger (SSH) model with the Hamiltonian[35,36]

$$\begin{aligned} H_{\rm m} =& \sum_{i,\sigma} -(t_0-\alpha y_i)\left(c^{\dagger}_{i+1,\sigma}c_{i,\sigma}+c^{\dagger}_{i,\sigma}c_{i+1,\sigma}\right) \\ &+\frac{K}{2}\sum_i (u_{i+1}-u_i)^2 - t_{\rm so}\sum_i (c^{\dagger}_{i+1,\uparrow}c_{i,\downarrow} \\ &-c^{\dagger}_{i,\uparrow}c_{i+1,\downarrow}+c^{\dagger}_{i,\downarrow}c_{i+1,\uparrow}-c^{\dagger}_{i+1,\downarrow}c_{i,\uparrow}). \end{aligned} \tag{1}$$

Here t_0 is the hopping integral of a uniform lattice and α stands for the e-l coupling strength. y_i is the lattice distortion with $y_i = u_{i+1}-u_i$. u_i is the lattice displacement of the ith site. $c^{\dagger}_{i,\sigma}(c_{i,\sigma})$ is the creation (annihilation) operator of π electrons at the ith site with spin σ, and K is the lattice elastic constant. $t_{\rm so}$ denotes the strength of the SOC.

The stable state of the organic chain can be obtained by solving the electronic eigenequations and lattice equilibrium equation self-consistently.[7] In Wannier space, the eigenstate can be expanded as $|\Psi_\mu\rangle = \sum_{i,\sigma}\psi_{\mu,i,\sigma}|i,\sigma\rangle$. $\psi_{\mu,i,\sigma}$ is the wave function at site i with spin σ. Thus, the eigenequation reads

$$\begin{aligned} &-(t_0-\alpha y_i)\,\psi_{\mu,i+1,\sigma}-(t_0-\alpha y_{i-1})\,\psi_{\mu,i-1,\sigma} \\ &-t_{\rm so}(\psi_{\mu,i-1,-\sigma}-\psi_{\mu,i+1,-\sigma}) = \varepsilon_\mu\psi_{\mu,i,\sigma}, \end{aligned} \tag{2}$$

where ε_μ is the eigenvalue. The lattice distortion y_i is recalculated by the lattice equilibrium equation

$$\begin{aligned} y_i =& -\frac{2\alpha}{K}\sum_{\mu,\sigma,\rm occ.}\psi_{\mu,i,\sigma}\psi_{\mu,i+1,\sigma} \\ &+\frac{2\alpha}{K(N-1)}\sum_{i=1}^{N-1}\sum_{\mu,\sigma,\rm occ.}\psi_{\mu,i,\sigma}\psi_{\mu,i+1,\sigma}, \end{aligned} \tag{3}$$

where N is the total site number in the chain and the sum is over all the occupied states. Equations (2) and (3) need to be solved self-consistently for a given occupied situation. Here, a fixed-end boundary condition is used.

When we investigate the transport properties of an organic device, two semi-infinite one-dimensional electrodes are connected to the left and right ends of the organic chain, as shown in Fig. 1. The electrode is described with the single-band tight-binding model with a spin splitting term[37]

$$\begin{aligned} H_{\rm FM} =& \sum_{i,\sigma}\left[\varepsilon_{\rm f}d^{\dagger}_{i,\sigma}d_{i,\sigma}+t_{\rm f}\left(d^{\dagger}_{i,\sigma}d_{i+1,\sigma}+d^{\dagger}_{i+1,\sigma}d_{i,\sigma}\right)\right] \\ &-\sum_i J_{\rm f}\left(d^{\dagger}_{i,\uparrow}d_{i,\uparrow}-d^{\dagger}_{i,\downarrow}d_{i,\downarrow}\right). \end{aligned} \tag{4}$$

Here, $\varepsilon_{\rm f}$ is the on-site energy relative to the atoms in the organic chain. $d^{+}_{i,\sigma}$ $(d_{i,\sigma})$ is the creation (annihilation) operator of the electron at ith site with spin σ. $t_{\rm f}$ is the hopping integral of electron and $J_{\rm f}$ represents the strength of the spin splitting. This model is usually adopted to describe a ferromagnetic metal due to the presence of the last Stoner-like spin-split term, but it can be also used for a nonmagnetic metal by setting $J_{\rm f}=0$. The interfacial coupling between the organic chain and the electrode is simplified as a hopping integral with $t_{\rm c} = \beta\,(t_{\rm f}+t_0)$. β is the weight parameter.

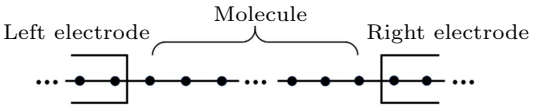


Fig. 1. Schematic diagram for the electrode/organic-chain/electrode device.

By applying a bias voltage, a uniform electric field is assumed to be generated along the organic chain. The Hamiltonian of the electric potential can be written as[38]

$$\begin{aligned} H_{\rm E} =& -\sum_{i,\sigma}|e|E\left[\left(i-\frac{N+1}{2}\right)a+u_i\right]c^{\dagger}_{i,\sigma}c_{i,\sigma} \\ &+\sum_i|e|E\left[\left(i-\frac{N+1}{2}\right)a+u_i\right], \end{aligned} \tag{5}$$

where e is the electron charge and $E = V/[(N-1)a]$ is the electric field generated from the bias voltage V. a is the lattice constant. Such treatment of the bias effect is valid when the bias is not too large.[39]

Under the bias voltage, the electronic structure and lattice configuration of the organic chain need to be recalculated by including the electric potential term in the eigenequations

and lattice equilibrium equation.[40,41] After that, the spin-resolved current can be calculated with the Landauer–Büttiker formula[42–44]

$$I_\sigma(V) = \frac{e}{h}\int T_\sigma(E,V)[f(E-\mu_{\rm L}) - f(E-\mu_{\rm R})]\,{\rm d}E. \quad (6)$$

Here h is Planck's constant. $T_\sigma(E,V)$ is the spin-dependent transmission function. In the presence of the SOC, the transmission includes both the spin-conserved component and the spin-flip one, i.e., $T_\sigma(E,V) = T_{\sigma\sigma}(E,V) + T_{-\sigma\sigma}(E,V)$. The spin-resolved transmission is calculated from $T_{\sigma\sigma'}(E,V) = {\rm Tr}[\Gamma^{\rm L}_\sigma G_{\sigma\sigma'}(E,V)\Gamma^{\rm R}_{\sigma'}G^{+}_{\sigma'\sigma}(E,V)]$. $\Gamma^{\rm L(R)}_\sigma = {\rm i}\left[\Sigma_{{\rm L(R)},\sigma} - \Sigma^{+}_{{\rm L(R)},\sigma}\right]$ is the broadening matrix due to the coupling with the ferromagnetic electrode.

$$G_{\sigma\sigma'}(E,V) = \frac{1}{E - H^{\rm e}_{\rm m} - \Sigma_{{\rm L},\sigma} - \Sigma_{{\rm R},\sigma}}$$

is the retarded single-particle Green's function of the central molecule, in which $H^{\rm e}_{\rm m}$ is the sum of the electronic parts in Eqs. (1) and (5). $f\left(E,\mu_{\rm L/R}\right)$ is the Fermi distribution function with the chemical potential $\mu_{\rm L/R} = E_{\rm F} \pm eV/2$. $E_{\rm F}$ is the Fermi energy of the electrode.

It is known that in spin valves the relative magnetization orientation of the two ferromagnetic electrodes may be parallel (P) or antiparallel (AP), manipulated by a magnetic field. The total charge current in each case is calculated as the sum of currents with different spins, $I = I_\uparrow + I_\downarrow$. The MR is defined as ${\rm MR} = (I_{\rm P} - I_{\rm AP})/I_{\rm AP}$ with $I_{\rm P}$ and $I_{\rm AP}$ the currents in P and AP configurations, respectively.

The parameters used for numerical calculations are chosen as follows. For the organic chain, $t_0 = 2.5$ eV, $\alpha = 4.1$ eV/Å, $K = 21.0$ eV/Å^2, which are typical values widely used for conjugated polymers such as polyacetylene.[45] For the ferromagnetic electrode, $t_{\rm f} = 1.5$ eV, $J_{\rm f} = 1.5$ eV, $\varepsilon_{\rm f} = -0.3$ eV, $E_{\rm F} = 0$, $\beta = 0.2$, which are used to fit the Co 3d band structure.[29] Despite that, the obtained results are expected to be valid qualitatively for other organic magnetic junctions. As mentioned earlier, the strength of SOC in organics depends on the components of the material and the molecular structure. For example, the SOC strength is 11 cm^{-1} for carbon atoms, and 382 cm^{-1} for S in sexithiophene and 112 cm^{-1} for Al in Alq_3.[16] Even in metal-free molecules, such as biphenyl, it has been reported that the SOC may be enhanced by four orders of magnitude by changing the angles between rings.[16] To make our results universal, here the SOC parameter is set as variable, while the dependence of results on the parameter is discussed.

3. Results and discussion

3.1. Spin admixture of eigenstates

Before the numerical calculation, we first derive the effect of SOC on the spin admixture of molecular eigenstates analytically. For the molecular chain, the electronic eigenstates will be spin degenerate with the absence of SOC, i.e., $E^0_{\upsilon,\uparrow} = E^0_{\upsilon,\downarrow}$. The corresponding eigenstates are $\left|\Psi^0_{\upsilon\uparrow}\right\rangle$ and $\left|\Psi^0_{\upsilon\downarrow}\right\rangle$. In the presence of SOC, the spin is not a good quantum number and each state contains components of the two spins. The new eigenfunctions, denoted by $\left|\Psi^+_\upsilon\right\rangle$ and $\left|\Psi^-_\upsilon\right\rangle$, can be calculated from the perturbation theory

$$\left|\Psi^+_\upsilon\right\rangle = \left|\Psi^0_{\upsilon,\uparrow}\right\rangle + \sum_{\mu\neq\upsilon}\frac{H^{\uparrow\downarrow}_{\rm so}}{E^0_\mu - E^0_\upsilon}\left|\Psi^0_{\mu,\downarrow}\right\rangle, \quad (7)$$

$$\left|\Psi^-_\upsilon\right\rangle = \left|\Psi^0_{\upsilon,\downarrow}\right\rangle + \sum_{\mu\neq\upsilon}\frac{H^{\downarrow\uparrow}_{\rm so}}{E^0_\mu - E^0_\upsilon}\left|\Psi^0_{\mu,\uparrow}\right\rangle. \quad (8)$$

Here $H^{\uparrow\downarrow}_{\rm so}$ ($H^{\downarrow\uparrow}_{\rm so}$) is the perturbation matrix between two spin components caused by the SOC Hamiltonian. In Wannier space, the perturbation matrixes are written as

$$\begin{aligned} H^{\downarrow\uparrow}_{\rm so} &= \sum_{i,j}\psi^0_{\upsilon,i\downarrow}\langle i,\downarrow| - t_{\rm so}\sum_n (c^\dagger_{n+1,\uparrow}c_{n,\downarrow} \\ &\quad - c^\dagger_{n,\uparrow}c_{n+1,\downarrow} + {\rm h.c.})\,|j,\uparrow\rangle\,\psi^0_{\mu,j,\uparrow} \\ &= -t_{\rm so}\sum_n[\psi^0_{\upsilon,n,\downarrow}\psi^0_{\mu,n+1,\uparrow} - \psi^0_{\upsilon,n+1,\downarrow}\psi^0_{\mu,n,\uparrow}], \quad (9) \\ H^{\uparrow\downarrow}_{\rm so} &= \sum_{i,j}\psi^0_{\upsilon,i\uparrow}\langle i,\uparrow| - t_{\rm so}\sum_n (c^\dagger_{n+1,\uparrow}c_{n,\downarrow} \\ &\quad - c^\dagger_{n,\uparrow}c_{n+1,\downarrow} + {\rm h.c.})\,|j,\downarrow\rangle\,\psi^0_{\mu,j,\downarrow} \\ &= -t_{\rm so}\sum_n[\psi^0_{\upsilon,n+1,\uparrow}\psi^0_{\mu,n,\downarrow} - \psi^0_{\upsilon,n,\uparrow}\psi^0_{\mu,n+1,\downarrow}]. \quad (10) \end{aligned}$$

Thus, the new eigenstates by considering the SOC are

$$\left|\Psi^+_\upsilon\right\rangle = \left|\Psi^0_{\upsilon,\uparrow}\right\rangle + \sum_{\mu\neq\upsilon}\frac{-t_{\rm so}\sum_n[\psi^0_{\upsilon,n,\downarrow}\psi^0_{\mu,n+1,\uparrow} - \psi^0_{\upsilon,n+1,\downarrow}\psi^0_{\mu,n,\uparrow}]}{E^0_\upsilon - E^0_\mu}\left|\Psi^0_{\mu,\downarrow}\right\rangle, \quad (11)$$

$$\left|\Psi^-_\upsilon\right\rangle = \left|\Psi^0_{\upsilon,\downarrow}\right\rangle + \sum_{\mu\neq\upsilon}\frac{-t_{\rm so}\sum_n[\psi^0_{\upsilon,n+1,\uparrow}\psi^0_{\mu,n,\downarrow} - \psi^0_{\upsilon,n,\uparrow}\psi^0_{\mu,n+1,\downarrow}]}{E^0_\upsilon - E^0_\mu}\left|\Psi^0_{\mu,\uparrow}\right\rangle. \quad (12)$$

According to these formulas, spin admixture of each eigenstate occurs caused by the SOC. The mixed component with opposite spin depends on not only the strength of SOC but also the initial wave functions and eigenvalues without SOC. The latter will be modified by the lattice configuration. Consequently, it leaves a way to modulate the SOC effect although the intrinsic atomic SOC of organics is weak because the lattice distortion is common in organics due to the strong e-l interaction, such as dimerization and polaron distortions.

In Wannier space, the eigenstates including the SOC between multiple eigenstates can be obtained numerically from the self-consistent calculation of Eqs. (2) and (3), which have the following form:

$$\left|\Psi_{\upsilon}^{+(-)}\right\rangle = \sum_{i} \psi_{\upsilon,i,\uparrow}^{+(-)} |i,\uparrow\rangle + \sum_{i} \psi_{\upsilon,i,\downarrow}^{+(-)} |i,\downarrow\rangle, \tag{13}$$

where $\psi_{\upsilon,i,\uparrow}^{+(-)}$ ($\psi_{\upsilon,i,\downarrow}^{+(-)}$) is the wave function. Here we define a spin admixture parameter of an eigenstate as

$$\gamma(\upsilon) = \frac{\gamma_{-\sigma}(\upsilon)}{\gamma_{\sigma}(\upsilon)} = \frac{\sum_{i} |\psi_{\upsilon,i,-\sigma}^{+(-)}|^2}{\sum_{i} |\psi_{\upsilon,i,\sigma}^{+(-)}|^2}$$

by the spin-resolved coefficient $\gamma_{\sigma}(\upsilon)$.

In the following, we first take the frontier highest occupied molecular orbital (HOMO) as an example to investigate the spin admixture effect. Here a lattice with 100 sites is adopted. The spin admixture is investigated in three cases: uniform, dimerized, and polaron chains. The uniform chain is achieved by setting the e-l interaction as zero, which is used to make a comparison with organic chains. The dimerized and polaron lattices are obtained by the self-consistent calculations mentioned above with nonzero α, where the electron occupation is half-filling or single-electron charged, respectively. In Fig. 2, we first plot the probability density of the HOMO for the three lattices with the SOC, specifically, the spin-up branch of the degenerated HOMOs. Without the SOC, delocalized orbitals are observed in the uniform and dimerized lattices, while a localized one appears in the polaron lattice due to the polaron lattice distortion. When t_{so} is nonzero, the spin-down component arises in the eigenstate, where the form of the probability density differs for the three lattices. The amplitude of the spin-down component increases with t_{so} and becomes comparable to the spin-up one at around $t_{so} = 0.04$ eV.

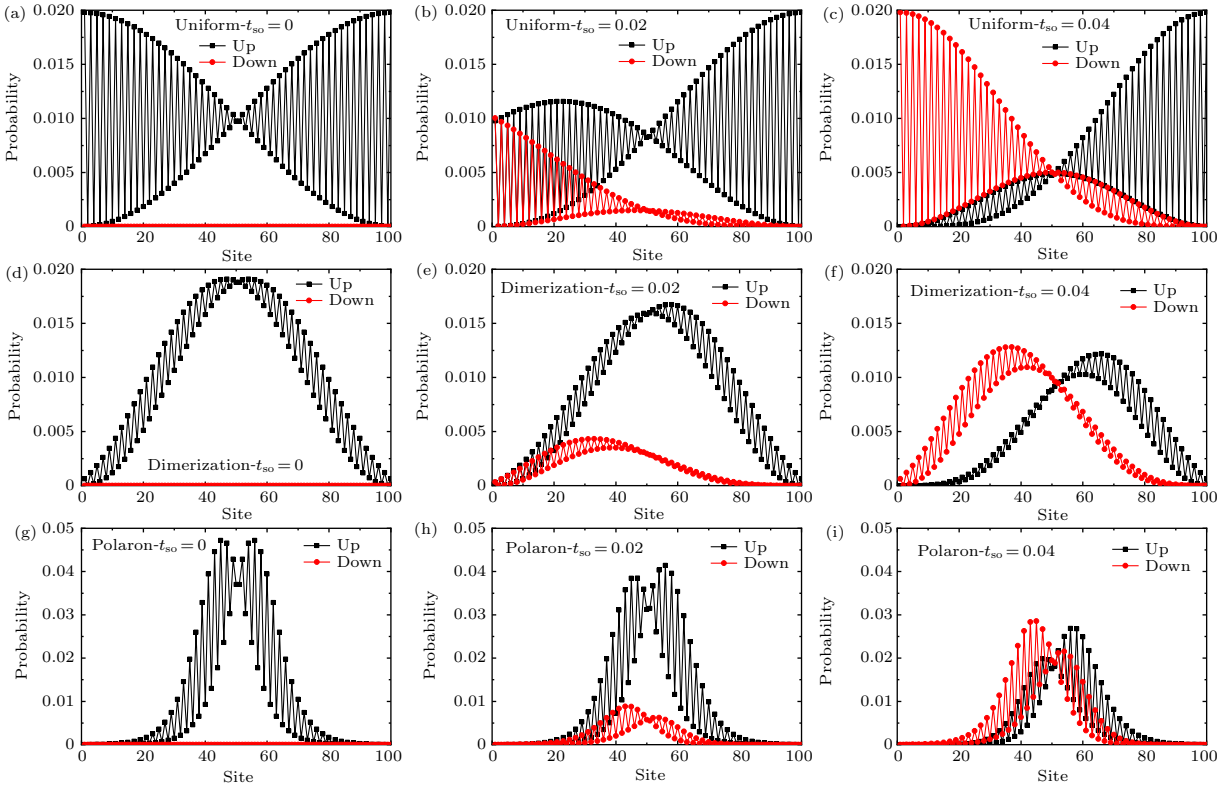


Fig. 2. Probability of the HOMO wave function at different SOC strengths and lattice configurations. (a)–(c) $t_{so} = 0$ eV, 0.02 eV, and 0.04 eV for uniform lattice. (d)–(f) $t_{so} = 0$ eV, 0.02 eV, and 0.04 eV for dimerized lattice. (g)–(i) $t_{so} = 0$ eV, 0.02 eV, and 0.04 eV for polaron lattice.

A quantitative investigation of the spin admixture can be achieved from the spin-resolved coefficient γ_{σ} and the spin admixture parameter γ. Figure 3 shows the changes in the two quantities of the HOMO with t_{so}. It is found that γ_{σ} changes non-monotonically with t_{so}. The mixed component with opposite spin increases quickly with t_{so}, and exceeds the initial spin component after $t_{so} = 0.04$ eV, and then begins to decrease. This leads to a peak for the spin admixture parameter γ at a specific value of t_{so} for different lattices. Below 0.04 eV of t_{so}, the spin admixture parameter γ shows little difference between the three lattices. However, when t_{so} is increased over 0.04 eV, we found that the spin admixture turns more distinct for the polaron lattice, where the maximum value achieves 8.5 at $t_{so} = 0.75$ eV. The dimerized lattice also has a larger γ than the uniform one, whose maximum value of 3.0 at $t_{so} = 0.65$ eV is two times that of the uniform lattice, only 1.5 at $t_{so} = 0.55$ eV. This means that the lattice distortion of dimerization or polaron may enhance the spin admixture of the frontier orbital,

but a relatively large t_{so} is required. To achieve a large t_{so}, a gate voltage or the presence of large atomic-number component will be necessary, such as S in thiophene with the SOC strength of 382 cm^{-1}, Al in Alq_3 of 112 cm^{-1}, and Cu in CuPc of 829 cm^{-1}.[16,46] Despite that, the role of lattice distortion on spin transport related to the SOC effect cannot be simply judged from the SOC strength. In our previous studies of polaron dynamics in two-dimensional organic lattices,[23,24] the lattice distortion contributes an extrinsic mechanism of skew scattering and enhances the spin Hall effect. So, in the following, we further investigate the spin-polarized quantum transport in organic devices in the presence of both SOC and lattice distortion.

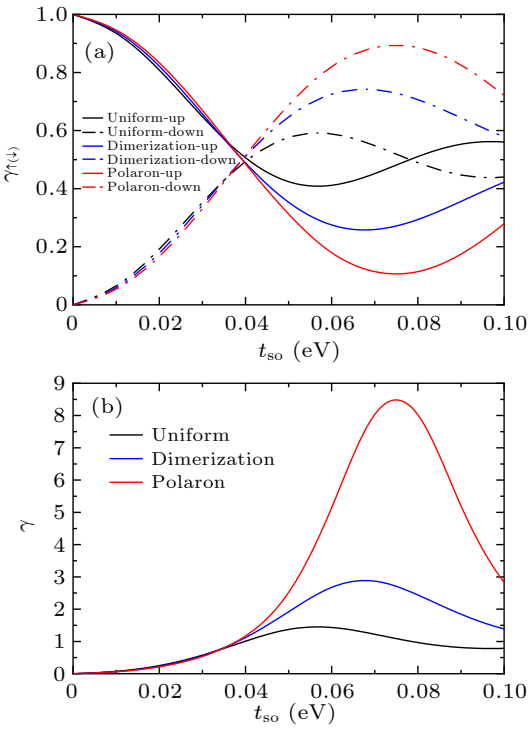


Fig. 3. (a) Spin-resolved coefficient $\gamma_{\uparrow(\downarrow)}$ and (b) spin admixture parameter γ of the HOMO in three lattices.

3.2. Electronic transport

We calculate the quantum transport properties of the above lattices in the presence of SOC by connecting them to electrodes, as illustrated in Fig. 1. A shorter chain of $N = 20$ is considered for quantum transport. First, two identical one-dimensional nonmagnetic electrodes are used, where the parameters are the same as those stated above except by setting $J_f = 0$. The transmission spectra of the three devices at zero bias are given in Fig. 4, where the results with and without SOC are compared. Here to make the results visible, a little larger SOC is used. It can be seen from Fig. 4(a) that the total transmission spectra keeps almost unchanged in the presence of SOC. But from Fig. 4(b) we can clearly find that a spin-flip transmission arises with SOC, where $T_{\uparrow\downarrow}$ and $T_{\downarrow\uparrow}$ overlap and the peak value achieves about 0.3. This is natural because the SOC will not break the spin degeneracy of the system.

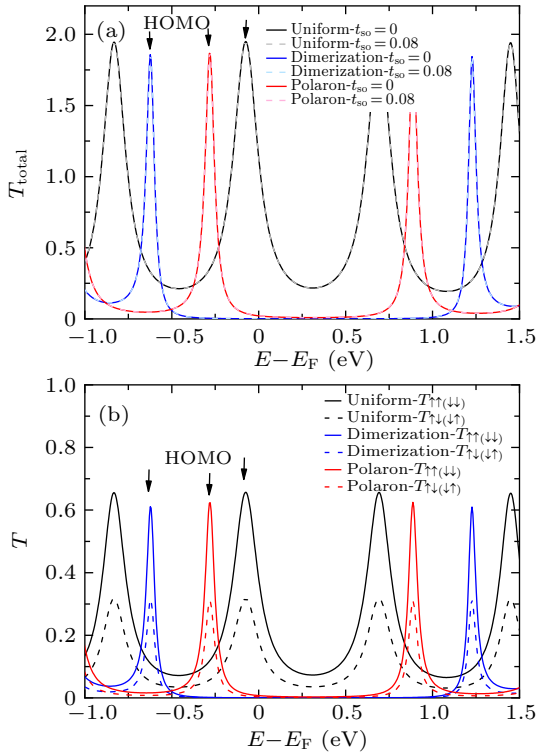


Fig. 4. (a) Transmission spectra through the three lattices with nonmagnetic electrodes. The solid lines represent for $t_{so} = 0$, and the dotted lines for $t_{so} = 0.08$ eV. (b) The spin-resolved transmission spectra in three cases with $t_{so} = 0.08$ eV.

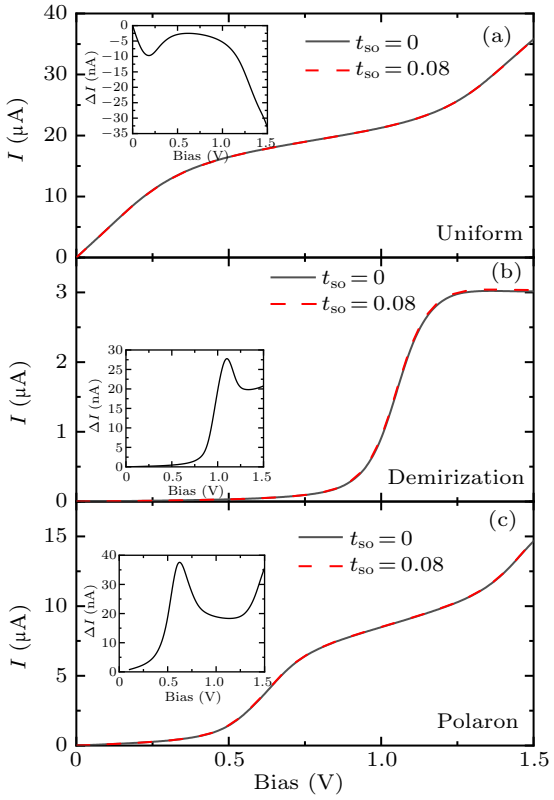


Fig. 5. Current as a function of the bias through the three devices with and without SOC in the case of nonmagnetic electrodes. Panels (a)–(c) correspond to uniform, dimerized and polaron chains, respectively. The insets are the difference of the currents with and without SOC, $\Delta I = I_{0.08} - I_0$.

We also calculated the current–voltage curves of the three devices. The results are shown in Fig. 5. It is found that the

lattice distortions modify the threshold voltage due to the modified energy gap. However, the change of current caused by SOC is in the order of thousandth for all cases, which is almost invisible in the curve. The insets show the difference of currents with and without SOC, which is in the order of nA for the present parameters. The change of current is a little larger in the polaron lattice. So, in present nonmagnetic electrodes, the effect of SOC on the current is insignificant and can be nearly ignored.

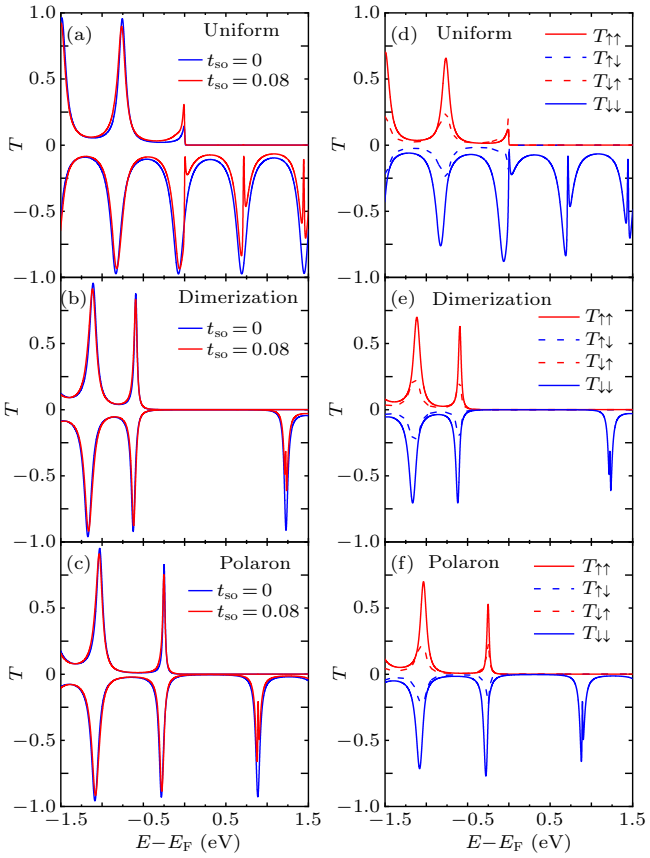


Fig. 6. Transmission spectra through the three lattices in the presence of ferromagnetic electrodes with $t_{so}=0$ eV and 0.08 eV. The magnetization orientations of the electrodes are parallel. Panels (a)–(c) are total transmission in uniform chain, dimerized chain, and polaron chain, respectively. The corresponding spin-resolved transmission spectra are given in (d)–(f).

Now we use two ferromagnetic metals as the electrodes. We start with the transmission spectra in P configuration of the electrodes. The parameters provided above generate a band structure similar to Co 3d states, which is composed of a full-filled majority band and a half-filled minority band. Thus, as shown in Figs. 6(a)–6(c), the spin-up (majority) transmission only exists below the Fermi energy. Unlike the nonmagnetic electrodes, the effect of SOC turns much stronger in this case, where the transmission peaks near the Fermi energy are reduced, especially for those spin-down peaks above the Fermi energy. This can be understood as follows. The SOC splits the total transmission into four components, $T_{\uparrow\uparrow}$, $T_{\downarrow\downarrow}$, $T_{\uparrow\downarrow}$, and $T_{\downarrow\uparrow}$. The magnitude of each transmission is related to the density of states (DOS) of the electrodes, e.g., $T_{\sigma\sigma'}(E) \propto \rho_{L,\sigma}(E)\rho_{R,\sigma'}(E)$. The spin-conserved transmission is from the majority (minority) to the majority (minority), while the spin-flip transmission at an energy E depends on the DOS of the two electrodes with different spins. Unlike the nonmagnetic electrode, in ferromagnetic metals the DOS of the majority and minority are not symmetric. Thus, once the SOC is included, the total transmission will differ from that without SOC. Especially for the transmission above the Fermi energy, as shown in Figs. 6(d)–6(f), the spin-flip transmission is forbidden because only spin-down states survive. This leads to a more notable change of the total transmission for these states, as shown in Figs. 6(a)–6(c). We also notice that a large Peierls energy gap appears for the dimerized and polaron lattices, which drives the frontier states away from the Fermi energy.

When the magnetization orientation of the two ferromagnetic electrodes is switched to AP alignment, the effect of the SOC on the transmission is also investigated, as shown in Fig. 7. For the HOMO transmission peak, it is found that the height is decreased significantly in the uniform lattice by the SOC, while only changes slightly in the presence of lattice distortions. At first glance the larger SOC effect in the uniform lattice seems contradictory to the conclusion mentioned above that the distortion enhances the SOC effect on spin admixture. This is because besides the spin admixture, the lattice dimerization also leads to an energy gap and drives the HOMO away from the Fermi energy, while the HOMO of the uniform lattice keeps close to the Fermi energy. As mentioned above, the effect of SOC on transmission is also related to the DOS of the electrodes. The asymmetry of DOS of the electrodes with different spins is the largest at the Fermi energy for Co, e.g., the center of the minority band versus the edge of the majority band. As a result, the transmission $T_{\downarrow\uparrow}$ caused by the SOC corresponds to a larger DOS at both the left and right electrodes, and thus a larger magnitude than the spin-conserved one. Such analysis can be confirmed by the spin-resolved transmission of the HOMO shown in Fig. 7(d), where a distinct spin-flip transmission peak is observed for the HOMO. In Figs. 7(e) and 7(f), the spin-flip transmission with lattice distortions is not as strong as in the uniform lattice, due to the separation of the HOMO to the Fermi energy, caused by the Peierls gap. Thus, in organic devices, the role of lattice distortions in the SOC effect may also embody in the modification of spin-resolved conducting states in electrodes, which will bring indirect contribution to the SOC effect, even more notable than the spin mixture of eigenstates.

Another remarkable change appearing in the antiparallel case is the rising spin-up transmission peaks above the Fermi energy, which are not observed in the absence of SOC. From Figs. 7(d)–7(f), such transmission peaks are contributed by the

spin-flip transmission part $T_{\downarrow\uparrow}$ because only spin-down (spin-up) states survive above the Fermi energy in the left (right) electrode. These transmission peaks are fully polarized, which means that spin filtering may be caused by the SOC in the involved energy range.

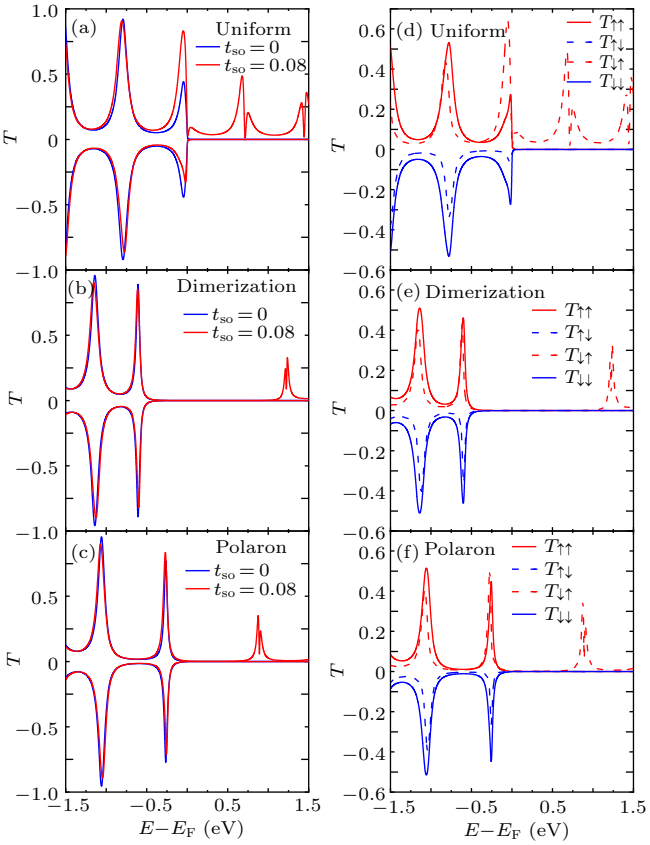


Fig. 7. Transmission spectra through the three lattices with antiparallel magnetization orientation of the two ferromagnetic electrodes.

The obvious change of transmission spectra at different magnetization orientations caused by SOC is expected to modify the current–voltage characteristic of the device, and even the MR. The current–voltage characteristic is first calculated and shown in Fig. 8. A more notable change is observed in the AP case, especially in the case of uniform lattice. This is consistent with the transmission spectra shown above, due to the larger conducting states of the electrodes for the uniform lattice. In the AP case, the current becomes larger in the presence of SOC, while it becomes smaller in the P case. This is because of the additional contribution of the spin-flip transmission above the Fermi energy in the AP case. So, the effect of SOC on the current relies on the relative magnetization orientation of the electrodes, while the lattice distortions suppress the change of current by modifying the conducting states.

In Fig. 9, we plot the dependence of MR on bias in the three devices with and without SOC. A decay of the MR with bias is observed in all cases, which is quite universal in organic spin valves. In the presence of SOC, the MR is suppressed for all devices compared with those without SOC, where the decreased amplitude is larger in the case of the uniform lattice at

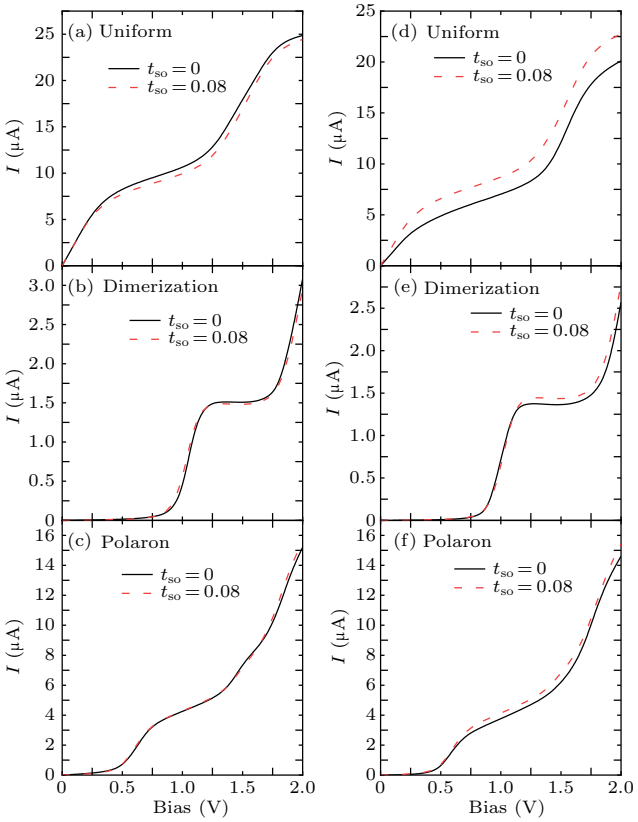


Fig. 8. Current as a function of the bias through the three devices with and without SOC. Panels (a)–(c) correspond to uniform, dimerized and polaron chains with parallel magnetization orientation of the electrodes. Panels (d)–(f) are those with antiparallel magnetization orientation of the electrodes.

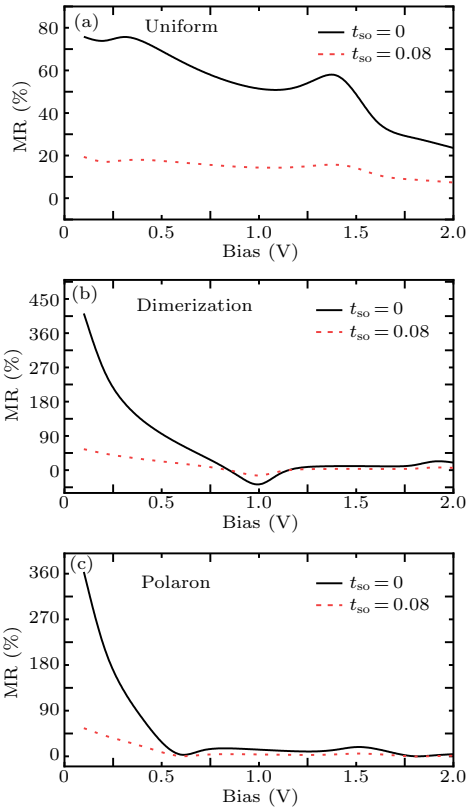


Fig. 9. Magnetoresistance as a function of bias in spin valves with and without t_{so}. (a) Uniform chain, (b) dimerized chain, and (c) polaron chain.

high bias. This is consistent with the distinct change of transmission for the uniform lattice shown above. At high bias, the value of MR remains at around 10% for the uniform lattice, while it tends to zero for the dimerized and polaron lattices. A remarkable drop of the MR for the latter two chains is only observed at low bias before the threshold voltage, where the current is too small and easily disturbed by the SOC.

4. Summary

With an extended SSH model, the effect of SOC on spin admixture of electronic eigenstates and spin-dependent transport in organic chains has been investigated. The role of lattice distortion induced by the strong e-l interaction in organics is focused. The results have been presented and compared with three types of chains, the uniform chain without e-l interaction, and the dimerized and the polaron chains with e-l interaction. By defining a spin admixture parameter, it is found that the spin admixture of frontier eigenstates changes non-monotonically with the strength of SOC. The e-l interaction induced lattice distortion may enhance the spin admixture of the eigenstates, where a relatively larger SOC is required. The role of lattice distortion in the SOC effect is analyzed by first-order perturbation theory, where the spin admixture depends on not only the strength of SOC but also the undisturbed wave functions and eigenvalues determined by the lattice configuration.

The effect of the SOC on the quantum transport property is investigated for nonmagnetic and ferromagnetic electrodes, respectively. For nonmagnetic electrodes, the total transmission and current are hardly affected by the SOC, although spin-flip transmission arises in the presence of SOC. But for ferromagnetic electrodes, the SOC effect turns more distinct, which further relies on the relative magnetization orientation of the electrodes. Spin filtering induced by spin-flip transmission is observed in the AP configuration. Decreasing of the MR caused by the SOC occurs, which is more notable for the uniform lattice. Unlike the spin admixture, the lattice distortion suppresses the SOC effect on the quantum transport. The reason is that the lattice dimerization drives the frontier orbital away from the Fermi energy by opening a Peierls energy gap, and thus modifies the valid spin-polarized conducting states in ferromagnetic electrodes, which further changes the spin-resolved transmission. The results mean that the lattice distortion may bring an indirect SOC effect on spin-dependent transport besides the spin mixture of the eigenstates. This work is helpful to understand the role of lattice distortion in the SOC effect on organic lattice, and may also be helpful for the future design of organic spin valves.

Acknowledgement

Project supported by the National Natural Science Foundation of China (Grant Nos. 11974215, 21933002, and 12274264).

References

[1] Li D and Yu G 2021 *Adv. Funct. Mater.* **31** 2100550
[2] Zhang H Q, Li D, Miao Y Y, Qiu S, Zhang G P, Ren J F, Wang C K, and Hu G C 2022 *Phys. Lett. A* **443** 128200
[3] Sun X, Bedoya-Pinto A, Mao Z, Gobbi M, Yan W, Guo Y, Atxabal A, Llopis R, Yu G, Liu Y, Chuvilin A, Casanova F and Hueso L E 2016 *Adv. Mater.* **28** 2609
[4] Zhu Y N, Jiang Q L, Zhang J and Ma Y G 2023 *Chem. Asian J.* **18** e202201125
[5] Meng K, Guo L D and Sun X N 2023 *Nanoscale Horiz.* **8** 1132
[6] Hu G C, Wei J H and Xie S J 2007 *Appl. Phys. Lett.* **91** 142115
[7] Hu G C, Zhang G P, Ren J F, Wang C K and Xie S J 2011 *Appl. Phys. Lett.* **99** 082105
[8] Zuo M Y, Hu G C, Li Y, Ren J F and Wang C K 2014 *Chin. Phys. B* **23** 087306
[9] Gobbi M and Orgiu E 2017 *J. Mater. Chem. C* **5** 5572
[10] Chen J, Fan G H, Zhang Y Y, Pang W, Zheng S W and Yao G R 2012 *Chin. Phys. B* **21** 058504
[11] Wei J H, Xie S J, Mei L M, Berakdar J and Yan Y J 2007 *Org. Electron.* **8** 487
[12] Wei J H, Xie S J, Mei L M, Berakdar J and Yan Y J 2006 *New J. Phys.* **8** 82
[13] Alotibi S, Hickey B J, Teobaldi G, Ali M, Barker J, Poli E, O'Regan D D, Ramasse Q, Burnell G, Patchett J, Ciccarelli C, Alyami M, Moorsom T and Cespedes O 2021 *ACS Appl. Mater. Interfaces.* **13** 5228
[14] Shafikov M Z, Zaytsev A V and Kozhevnikov V N 2021 *Inorg. Chem.* **60** 642
[15] Sun D, Zhang C, Kavand M, Wang J, Malissa H, Liu H, Popli H, Singh J, Vardeny S R, Zhang W, Boehme C and Vardeny Z V 2019 *J. Chem. Phys.* **151** 174709
[16] Yu Z G 2012 *Phys. Rev. B* **85** 115201
[17] Jiang H, Zhang C, Hu X N, Hu G C and Xie S J 2015 *Mod. Phys. Lett. B* **29** 1450266
[18] Bercioux D and Lucignano P 2015 *Rep. Prog. Phys.* **78** 106001
[19] Liang S, Geng R, Yang B, Zhao W, Chandra Subedi R, Li X, Han X and Nguyen T D 2016 *Sci. Rep.* **6** 19461
[20] Zhang L L, Hao Y Y, Qin W, Xie S J and Qu F Y 2020 *Phys. Rev. B* **102** 214303
[21] Maslyuk V V, Gutierrez R, Dianat A, Mujica V and Cuniberti G 2018 *J. Phys. Chem. Lett.* **9** 5453
[22] Liu F 2023 *Coshare Science* **01** v3 p1–62
[23] Hu G C, Miao Y Y and Timm C 2022 *Phys. Rev. B* **106** 144309
[24] Miao Y Y, Li D, Zhang H Q, Ren J F and Hu G C 2023 *Phys. Chem. Chem. Phys.* **25** 7763
[25] Miao Y Y, Zhang H Q, Ma H, Li H X, Ren J F and Hu G C 2024 *Phys. Rev. B* **109** 014314
[26] Nuccio L, Willis M, Schulz L, Fratini S, Messina F, D'Amico M, Pratt F L, Lord J S, McKenzie I, Loth M, Purushothaman B, Anthony J, Heeney M, Wilson R M, Hernández I, Cannas M, Sedlak K, Kreouzis T, Gillin W P, Bernhard C and Drew A J 2013 *Phys. Rev. Lett.* **110** 216602
[27] Xu F, Li B, Pan H and Zhu J L 2007 *Phys. Rev. B* **75** 085431
[28] Fallah F and Esmaeilzadeh M 2011 *AIP Adv.* **1** 032113
[29] Vetter E, VonWald L, Yang S J, Yan L, Koohfar S, Kumah D, Yu Z G, You W and Sun D 2020 *Phys. Rev. Mater.* **4** 085603
[30] Sierra M A, Sanchez D, Gutierrez R, Cuniberti G, Dominguez-Adame F and Diaz E 2019 *Biomolecules* **10** 49
[31] Baronas P, Komskis R, Tankeleviciu Te E, Adomenas P, Adomeniene O and Jursenas S 2021 *J. Phys. Chem. Lett.* **12** 6827
[32] Gutierrez R, Láz E, Naaman R and Cuniberti G 2012 *Phys. Rev. B* **85** 081404

[33] Jana M K, Song R, Liu H, Khanal D R, Janke S M, Zhao R, Liu C, Valy Vardeny Z, Blum V and Mitzi D B 2020 *Nat. Commun.* **11** 4699
[34] Naderi F and Hasanirokh K 2020 *Prog. Theor. Exp. Phys.* **2020** 073I01
[35] Su W P, Schrieffer J R and Heeger A J 1979 *Phys. Rev. Lett.* **42** 1698
[36] Wang X F and Chakraborty T 2006 *Phys. Rev. B* **74** 193103
[37] Xie S J, Ahn K H, Smith D L, Bishop A R and Saxena A 2003 *Phys. Rev. B* **67** 125202
[38] Miao Y Y, Qiu S, Zhang G P, Wang C K, Ren J F and Hu G C 2021 *Physica E* **131** 114729
[39] Hu G C, Zuo M Y, Li Y, Ren J F and Xie S J 2014 *Appl. Phys. Lett.* **104** 033302
[40] Fang Z, Liu Z L and Yao K L 1994 *Phys. Rev. B* **49** 3916
[41] Hu G C, Guo Y, Wei J H and Xie S J 2007 *Phys. Rev. B* **75** 165321
[42] Landauer R 2006 *Philos. Mag.* **21** 863
[43] Datta S 1995 *Electronic Transport in Mesoscopic Systems* (New York: Oxford University Press)
[44] Paulsson M, Brandbyge M 2007 *Phys. Rev. B* **76** 115117
[45] Zuo M Y, Hu G C, Li Y, Ren J F and Wang C K 2014 *Chin. Phys. B* **23** 087306
[46] Lei J, Li H, Yin S and Xie S J 2008 *J. Phys.: Condens. Matter* **20** 095201